PCCP

Accepted Manuscript

ROYAL SOCIETY OF CHEMISTRY

rsc.li/pccp

View Article Online
DOI: 10.1039/C7CP05266A

A ring polymer molecular dynamics study of the OH + H_2(D_2)reaction.

J. F. Castillo [a*] and **Y. V. Suleimanov**[b,c]

In this work we have performed a ring polymer molecular dynamics (RPMD) study of the OH + H_2 and OH + D_2 reactions at temperatures ranging from 150 K to 2000 K using two available *ab initio* potential energy surfaces (PESs) that have been termed as the YZCL2 and NN1 PES, respectively. The YZCL2 PES was developed by Yang *et al.* [*J. Chem. Phys.*, 2001, **115**(1), 174] which is based on points fitted by a modified shephard interpolation method and calculated with unrestricted coupled-cluster theory with all single and double excitations and a perturbative account of triple excitations (UCCSD(T)) method with an aug-cc-pVQZ basis. The NN1 PES was constructed by Chen *et al.* [*J. Chem. Phys.*, 2013, **138** (15), 154301] using a neural networks method to fit *ab initio* energies calculated at UCCSD(T)- F12a/AVTZ level of theory. We show that both techniques provide reliable PESs. The RPMD thermal rate coefficients and the kinetic isotope effects (KIEs) calculated using these two PESs are in very good agreement with each other as well as with the previous experimental values available to the date. Besides, we have shown that these two procedures for fitting PESs can yield even more similar RPMD rate coefficients when the same level of *ab initio* theory is employed, at least for the present OH + H_2 reaction. Comparison with the previous theoretical calculations on the NN1 PES, namely, instanton theory and canonical variational theory with microcanonical optimized multidimensional tunneling, shows that the present RPMD results are more consistent and accurate. Future experimental measurements of the KIEs and accurate quantum mechanical calculations on these PESs are highly desirable, especially at low temperatures.

1 Introduction

The reaction

$$\mathrm{OH}(^2\Pi) + \mathrm{H_2} \rightarrow \mathrm{H} + \mathrm{H_2O} \qquad \Delta_r H_0^o = -16.3 \text{ kcal mol}^{-1} \tag{1}$$

is considered as a prototype reaction for four-atom systems which involves three Hydrogen atoms and therefore amenable of high quality *ab initio* quantum chemical and dynamical studies. In addition to its theoretical interest it is of considerable practical importance since it occurs in the chain propagation steps of hydrogen combustion[1] and atmospheric chemistry processes[2]. Besides the reaction is thought to take place in the shock chemistry of interstellar clouds[3] and in the formation of H_2O on interstellar grains[4]. As a consequence, it has been the object of many experimental and theoretical investigations that has been reviewed several times[5–7]. More relevant to this work are the kinetic bulk experiments that have measured rate coefficients over an extended range of temperatures[2,8–14]. Interestingly the Arrhenius plot of the rate coefficient exhibits a nonlinear profile with a pronounced curvature at 300 K and below. Such a behavior is the fingerprint of atom quantum tunneling through the reaction barrier. The sets of experimental data can be fitted to a modified Arrhenius expression of the form[9]

$$k(T) = A\, T^B\, exp(-C/T) \tag{2}$$

the data in the temperature range of 250-1050 K measured by Tully *al.*[9] yielded A = 4,12 $\times$ 10^{-19} cm^3 s^{-1} , B = 1,44 and C = 1281 K for reaction OH + H_2 and A = 4,37 $\times$ 10^{-15} cm^3 s^{-1} , B = 1,18 and C = 2332 K for reaction OH + D_2 . A

[a] *Departamento de Química Física I, Facultad de CC. Químicas, Universidad Complutense de Madrid, 28040 Madrid, Spain.*
[b] *Computation-based Science and Technology Research Center, Cyprus Institute, 20 Kavafi Street, Nicosia 2121, Cyprus*
[c] *Department of Chemical Engineering, Massachusetts Institute of Technology, Cambridge, Massachusetts 02139, United States*
* Email:jfernand@ucm.es

View Article Online
DOI: 10.1039/C7CP05266A

set of rate coefficients were measured by Michael and Sutherland[10] between 1246-2581 K and by Oldengorg and coworkers[12] between 800-1550 K. The above sets of data were fitted[12] with A = 3,56 $\times$ 10^{-16} cm^3 s^{-1} , B = 1,52 and C = 1736 K for reaction $OH + H_2$ in the temperature range of 250-2581 K. Despite of the non-Arrhenius behaviour of the rate coefficients the experimental activation energies can be approximately established as 0.17 eV for $OH + H_2$, and 0.23 eV for $OH + D_2$.

There have been numerous theoretical studies in order to attempt to reproduce the extensive and accurate kinetic data that are available from experiments on reaction (1). During the 80's and early 90's, most of these efforts made use of an *ab initio* potential energy surface (PES), constructed by Schatz and Elgersma[15], named as WDSE PES and that is now known to be not very accurate and has been superseded by newer global PES's. Canonical variational theory (CVT) was applied by Isaacson and Truhlar [16] in order to calculated rate coefficients for the $OH + H_2$ and $OH + D_2$ using the WDSE PES. Full-dimensional time independent quantum mechanical (TIQM) calculations of the rate coefficients employing the WDSE PES were performed by Manthe *et al.*[17,18] yielding results significantly larger than the experimental values (a factor of 4 at 300 K). More recent full-dimensional time dependent quantum mechanical (TDQM) on the same PES carried out by Yang *et al.*[19] confirmed that the WDSE PES lead to an overestimation of the measured rate coefficients. A very large computational effort was undertaken by Yang, Zhang, Collins and Lee that culminated in the construction of a global PES. Such surface, termed the YZCL2 PES[19], is calculated by a modified Shephard interpolation of a set of 2000 UCCSD(T)/aug-cc-pVQZ energies, gradients and hessians. The same authors employed the TDQM method to calculate rate coefficients in the 250-1050 interval[19] that were found to be in very good agreement with the experimental results. Another global *ab initio* PES was constructed by Wu *et al.*, the WSLFH PES[20], and used by Chakraborty and Truhlar[21] in TIQM calculations of the rate coefficients with good agreement with TDQM calculations[22] and experimental determinations. Better agreement with the experimental values was achieved by Nguyen *et al.*[23] by applying semiclassical transition-state theory (SCTST) in combination with VPT2/CCSD(T) *ab initio* calculations. At 200 K, they underestimate the experimental rate coefficient by a factor of 1.43, which is comparable to the experimental error bar. The most recent global PES to date has been developed using Neural Networks (NN) fitting of 17000 UCCSD(T)-F12a/AVTZ data by Chen *et al.*[24] (NN1 PES). Reaction rate coefficients of (1) down to 100 K using instanton semiclassical theory and down to 50 K using canonical variational theory with microcanonical optimized multidimensional tunneling (CVT/μOMT) on the NN1 PES for all H/D isotopologues have been computed by Meisner and Kastner[25].

In this work, we have aimed to compute thermal rate coefficients of the title reaction using ring polymer molecular dynamics (RPMD) method[26,27] that has proven to give excellent results for gas–phase bimolecular reactions. This technique is capable of describing quantum effects such as tunneling and zero–point energy (ZPE). The RPMD method has been successfully applied to a variety of reactions with different reaction pathways [28–50] in a wide temperature range from classical high-temperature limit, where RPMD converges to classical MD, to low-temperature deep tunneling regime where RPMD is related to instanton theory[51] and to quantum transition state theory[52], as outlined in the recent review of RPMD rate theory and its practical applications[27].

In this work, the thermal rate coefficients for the $OH + H_2 \rightarrow H + H_2O$ reaction have been computed using the RPMD technique for temperatures ranging from 150 K to 2000 K using the YZCL2 and NN1 PES. Additionally, we assess the performance of the interpolation method in comparison with the NN technique for fitting *ab initio* points calculated at the same level of theory. Therefore we have constructed a new PES using the modified Shephard interpolation approach implemented in the Grow package[53] at the UCCSD(T)- F12a/AVTZ level of theory using MOLPRO[54]. The results have been compared with previous quasiclassical trajectory (QCT)[55], quantum mechanical (QM) and semiclassical calculations and with the experimental data available. The present paper is organized as follows: in Section 2 computational details of the calculations are described, results are shown and discussed in Section 3 and final conclusions are exposed in Section 4

View Article Online
DOI: 10.1039/C7CP05266A

2 Methodology

2.1 Details of RPMD calculations

RPMD calculations have been performed using the RPMDrate code[33]. Analysis of the RPMD theory applied to the calculation of gas phase bimolecular rate coefficients can be found in the recent review by one of us (YVS)[27].

In brief, the Bennett-Chandler factorization[56,57] is used which splits the calculation in two steps – (1) the construction of ring polymer potential of mean force W(ξ) (PMF or free energy) profile along the dimensionless reaction coordinate ξ (defined using the formalism of two dividing surfaces that connect the reactant (ξ = 0) and transition state regions (ξ = 1)[33]) and (2) the ring polymer transmission coefficient κ (TC or recrossing factor) calculation. These steps are usually performed consequently in order to detect the maximum value of W($\xi^{\#}$) during the first step and to initiate the calculations of κ from this point $\xi^{\#}$ during the second step. This allows minimizing recrossings (in order to avoid the issue of converging small values of κ due to an exponential sensitivity to ξ) and optimizing the propagation time required to achieve the plateau value of κ. For thermally activated energy profiles, the free energy barrier $\xi^{\#}$ is located near the classical saddle point configuration (ξ = 1)[27].

For the calculation of the PMF profiles, we divide the interval $\xi \in [-0.05, 1.05]$ in windows of width 0.01. In each window we perform 200 constrained RPMD trajectories of 100 ps of which the first 20 ps are used for thermalization. The time step was set to 0.0001 ps. The constrain that we apply at the window centered at ξ_i consists on adding a harmonic potential of the type $K(\xi - \xi_i)^2$ to the hamiltonian of the system, so that the trajectory explores only the vicinity of ξ_i. The value of the force constant K must be chosen big enough to just explore the surroundings of ξ_i and at the same time small enough to allow big overlapping between neighbouring ξ distributions. With the first two moments of the ξ distribution at each window, $\langle \xi_i \rangle$ and $\langle \xi_i^2 \rangle$, we can apply a thermodynamic integration scheme[58,59] to compute the centroid–density quantum transition state theory (QTST) rate coefficient. We will denote k_{QTST} for the present QTST calculations.

To obtain the TC, κ, we run trajectories which start at $\xi^{\#}$, which corresponds to the maximum of the PMF, as indicated above. In order to have a substantial sampling of initial conditions, a long trajectory of 2 ns is run after a thermalization period of 20 ps in the presence of an Andersen thermostat[60], with the constrain of having its centroid pinned at $\xi = \xi^{\#}$. Once every 2 ps the configuration of this *parent* trajectory is taken as the initial condition for 10000 *child* trajectories. All these child trajectories are run for 0.05 ps with different initial momenta and without either the constrain or the thermostat, to accumulate the TC. Once the TC κ is obtained, the RPMD rate coefficient k_{RPMD} is calculated as $k_{\mathrm{RPMD}} = \kappa \times k_{\mathrm{QTST}}$.

Table 1 Convergence of k_{QTST}, κ and k_{RPMD} with the number of beads at T=200 K . Rate coefficients are given in $10^{-15}\mathrm{cm}^3\mathrm{s}^{-1}$. Spin-orbit correction has not been applied.

N_{beads}	k_{QTST}	κ	k_{RPMD}
NN1 PES			
96	2.70	0.36	0.962
128	2.75	0.35	0.963
196	2.76	0.35	0.964
YZCL2 PES			
32	2.11	0.36	0.76
48	2.86	0.36	1.03
64	2.87	0.36	1.03
80	2.88	0.36	1.04

View Article Online
DOI: 10.1039/C7CP05266A

Calculations on the NN1 PES were carried out using 48 ring polymer beads at high temperatures and up to 128 beads for temperatures below 200 K. For the YZCl2 PES we employed 48 beads at high temperatures and 80 beads for T below 200 K. The convergence of k_{QTST}, κ and k_{RPMD} with the number of beads at T=200 K is shown in Table 1.

As we mentioned in the introduction, it would be interesting to assess the reliability and efficiency of the interpolation method employed for the YZCL2 PES in comparison withe the NN1 PES. For this purpose a new PES has been build using the Grow package[53] using the same level of theory as the NN1 PES, namely the UCCSD(T)-F12a/AVTZ theory. Such PES, denoted as UCCSD(T)-F12a/AVTZ INT PES, has been constructed in a first stage with a few points along the reaction path. Then the PES is refined iteratively by sampling points along the RPMD one bead trajectories on the different windows in the interval $\xi \in [-0.05, 1.05]$. Convergence of the RPMD coefficients in the considered temperature range has been obtained with 200 *ab initio* points. In Table 2 RPMD rate coefficients calculated on the three different PESs employed in this work are presented at two temperatures.

Table 2 RPMD rate coefficients (k_{RPMD}) for the $OH + H_2 \rightarrow H + H_2O$ reaction with different PESs . Rate coefficients are given in cm^3s^{-1}.

PES	1000 K	300K
UCCSD(T)/AVQZ YZCL2	$3{,}72 \times 10^{-12}$	$1{,}12 \times 10^{-14}$
UCCSD(T)-F12a/AVTZ NN1	$3{,}75 \times 10^{-12}$	$1{,}25 \times 10^{-14}$
UCCSD(T)-F12a/AVTZ INT	$3{,}70 \times 10^{-12}$	$1{,}15 \times 10^{-14}$

As can be seen, the RPMD coefficients from the three PESs are in very good agreement. Note that the new constructed INT PES improves the speed of gradients and energy evaluations of the interpolation algorithm in comparison with the YZCL2 PES because it required fewer *ab initio* points (the INT PES is based on 200 points whereas the YZCL2 PES contains 2000 points). However, the NN algorithm is faster than the interpolation code for the present system. Nevertheless, a main goal of this work is to calculate the rate coefficients on the PESs available on the literature that have employed in previous studies so the following results have been obtained using the YZCL2 and NN1 PESs.

3 Results and discussion

In Fig. 1 RPMD PMF profiles W(ξ) for 300 K and 1000 K are shown. The RPMD free energy barriers increase with temperature as expected. For all the temperatures studied, the PMFs are consistently close for the NN1, YZCL2 and our new UCCSD(T)-F12a/AVTZ INT interpolated PESs, the differences is small and does not exceed 0.01 eV though it contributes exponentially to the total RPMD thermal rate. Selected RPMD time-dependent TCs at 300 K and 1000 K are shown in Fig. 2. TCs decrease with decreasing the temperature in line with the previous RPMD simulations of thermally activated chemical reactions (see Ref.[27]). The difference between TCs obtained using the NN1 and YZCL2 and the UCCSD(T)- F12a/AVTZ interpolated PESs is again small, within convergence and contributes only linearly to the total RPMD thermal rate. In order to compare with the experimental rate coefficients[9,11–13], it is necessary to take OH spin–orbit coupling effects into account, which are not included in NN1 and YZCL2 PESs used in our RPMD calculations. The $^2\Pi_{1/2}$ excited state of OH, which is only Δ = 140 cm^{-1} above the $^2\Pi_{3/2}$ ground state can be included by considering that the ratio of transition state to reactant electronic partition functions adds a factor $\mathrm{F}(T)$, as in previous theoretical studies[16,17,21], in the following form

$$\mathrm{F}(T) = 1 + \ e^{-\Delta/\mathrm{k_B}T}. \tag{3}$$

The resulting spin—orbit corrected rate coefficient is $k^{\mathrm{corr}}_{\mathrm{RPMD}}(T) = \mathrm{F}^{-1}(T) \times k_{\mathrm{RPMD}}(T)$.

View Article Online
DOI: 10.1039/C7CP05266A

The comparison of the spin–orbit corrected RPMD rate coefficients for OH + H_2 with the experimental values and previous theoretical calculations is shown in Fig. 3. The low-temperature rate coefficients are also summarized in Table 3. One can first notice that the difference between RPMD rate coefficient for NN1 and YZCL2 is practically invisible except at very low temperature 150 K where it achieves 25% and can be attributed to convergence error due to more demanding low-temperature RPMD calculations thus demonstrating extremely good agreement between two PESs.

The RPMD results from both PESs, YZCL2 and NN1, are in very good agreement with the experimental determinations across all temperature range available for comparison. In the high-temperature limit, RPMD rates are significantly lower than the CVT/μOCT counterparts obtained with the NN1 PES. This can be attributed to the issues of transition state theory approaches with the proper treatment of the classical recrossing effects as discussed previously in Ref.[27]. In the YZCL2 case, the present RPMD rates can be compared with the previous QCT results[55] which demonstrate exemplary agreement with the present RPMD rate coefficients in the high-temperature limit but decrease too fast with decreasing temperature, apparently due to the inability by the QCT method of including tunneling and zero-point-energy effects along the reaction coordinate[27].

In the low-temperature limit, the discrepancy between CVT and RPMD results for the NN1 PES increases which can be attributed to less accurate treatment of tunneling effect by the former method as observed in the previous comparison[27]. In the YZCL2 case, QCT "switches" from agreeing with the RPMD rate coefficients at high temperatures to being lower than RPMD due to ignoring the contribution of the tunneling effect. Comparison with the instanton theory results for the NN1 PES is more tricky due to very limited available data. Note that, according to the previous studies,[27,32] the chemical reaction (1) with $\Delta_r H_0^o$ = -16.3 kcal mol^{-1} can be considered as "energetically asymmetric" and therefore RPMD is expected to overestimate the rate coefficients in this regime by a factor of no more than 2-3 (below the "crossover" temperature which is 276.2 K and 272.9 K for OH + H_2 on the NN1 and YZCL2 PESs, respectively). However, in certain cases, RPMD can be very accurate at low temperatures thus not exhibiting significant overestimation, see, for instance, Ref.[61]. Reverting to the present system, one observes that the instanton rate coefficient is higher than the RPMD one at 200 K by less than 10 % (see Table 3, barely visible in Fig. 3) but is lower at 150 K by 70 %. Since both 200 and 150 K are below the crossover temperature, it is not clear which method provides more accurate results for the present system in the deep tunneling regime. It is also worth noting that the previous comparison between the instanton and RPMD theories for gas-phase systems, for which rigorous quantum mechanical calculations in the deep tunneling regime were available for the same PESs, has demonstrated that RPMD is more accurate and reliable. This includes such systems as energetically asymmetric H + CH_4 reaction[30], in which "quantum" version of the instanton theory was systematically higher than RPMD and quantum mechanical results, and symmetric D + MuH chemical reactions[36], in which the semiclassical instanton theory exhibited irregular dependence with temperature and was also less accurate. Clearly, the rigorous quantum mechanical calculations of the low-temperature rate coefficients for the title system using the NN1 PES are highly desirable for proper and less speculative comparative analysis. In addition, more detailed comparison between RPMD and instanton theory results for other chemical reactions (supported by either quantum mechanical results for a given PES or by accurate PES calculations and experimental data) is also required in future.

Comparison with the other methods presented in Fig. 3 is less informative due to different PESs employed in these previous calculations. Nevertheless, it is worth noting excellent agreement between the experiment and the SCTST calculations performed by Nguyen *et al.*[23] on PES obtained with high-level CCSD(T)/ANO1 quantum chemistry. Even at 200 K the underestimation by SCTST (40 %) is comparable to the experimental error. Despite its TST's "no recrossing" assumption, SCTST approximation (usually applied to second-order vibrational perturbation theory)[62] provides very good estimates to the rate coefficients as it includes several important features such as non-empirical treatment of tunneling along multidimensional reaction path, intrinsic anharmonicity of the reaction coordinate and coupling of the reaction coordinate to the orthogonal bound degrees of freedom. However, its performance for very anharmonic transition states or in the deep tunneling regime can be problematic.[62] Unfortunately, detailed comparison between RPMD and SCTST is still missing partially due to the necessity to construct full-dimensional

View Article Online
DOI: 10.1039/C7CP05266A

PESs for RPMD dynamics and local direct-dynamics in the SCTST approach. In future, it will be very beneficial to address this lack of comparative study of these two methods.

In Fig. 4 RPMD rate coefficients from the NN1 and YZCL2 PESs are compared with experimental measurements, instanton and CVT/μOCT theoretical determinations for the $OH + D_2$ reaction. The QCT rate coefficient at room temperature (298 K) obtained using the YZCL2 PES is also included. As in the $OH + H_2$ case, the low-temperature rate coefficients are given in Table 3. Fig. 4 shows that RPMD rate coefficients are in a very good agreement with the experimental results slightly underestimating them but demonstrating proper curvature on the Arrhenius plot. Similar to $OH + H_2$ the difference between the RPMD results on two surfaces is practically negligible and confirms that both surfaces produce very similar results in RPMD studies. As in the $OH + H_2$ case, the CVT/μOCT overestimates the rates at all temperatures with stronger deviations at the highest (1000 K) and the lowest (250 K) temperatures available for comparison. The QCT is in a very good agreement with experiment at room temperature though comparison of a single result is not conclusive for proper method assessment. Instanton results obtained below the crossover temperature exhibit nonsystematic behavior being much higher than RPMD at $\sim$200 K but rapidly approaching RPMD at 150 K – opposite behavior compare to the $OH + H_2$ reaction (see Table 3). As a result, the instanton curvature on the Arrhenius plot at low temperatures is inconsistent with RPMD one as well as with the experimental temperature dependence at higher T.

Fig. 5 presents the kinetic isotope effect (KIE) for $k(T)_{(OH+H_2)}/k(T)_{(OH+D_2)}$. It shows that RPMD and experimental results are in very good agreement within the temperature range available for comparison (1000 - 250 K). At lower temperatures, the RPMD KIE increases significantly due to the tunneling effect of the H-transfer in the $OH + H_2$ reaction and is within the values obtained previously for OH + CH_4/CD_4 system[34]. However, from the previous RPMD studies[27,34], we expect RPMD to overestimate the KIE for the title reaction by a factor of two in the low-temperature limit. According to Fig. 5, the estimations by the instanton theory can be more reliable at low temperatures, however, as we discussed the instanton rate coefficients' different behavior for H_2 and D_2, more likely this originates from an error cancellation rather than from systematically more accurate behavior of the instanton theory as compared to RPMD. Again, quantum mechanical calculations of the low-temperature rate coefficients for both isotope combinations would be helpful for proper comparison of these two approaches.

In summary, RPMD results are in very good agreement with all experimental data available for comparison and exhibit reliable and systematic behavior as compared to some of the previous theoretical results. Further experimental KIE studies for the title reactions as well as rigorous quantum mechanical calculations at low temperatures will be very useful.

View Article Online
DOI: 10.1039/C7CP05266A

Table 3 Rate coefficients for the $OH + H_2$ and $OH + D_2$ reactions. Rate coefficients are given in cm^3s^{-1}. [a] This work. [b] Ref.[25], [c] Ref.[23], [d] Ref.[21], [e] Ref.[55], [f] Ref.[9], [g] Ref.[13]

$OH + H_2$ reaction				
Method	PES	300 K	200 K	150 K
RPMD[a]	UCCSD(T)/AVQZ YZCL2	$7{,}22 \times 10^{-15}$	$7{,}30 \times 10^{-16}$	$1{,}37 \times 10^{-16}$
RPMD[a]	UCCSD(T)-F12a/AVTZ NN1	$8{,}28 \times 10^{-15}$	$7{,}06 \times 10^{-16}$	$1{,}73 \times 10^{-16}$
Instanton[b]	UCCSD(T)-F12a/AVTZ NN1		$7{,}56 \times 10^{-16}$	$1{,}02 \times 10^{-16}$
CVT/μ OCT[b]	UCCSD(T)-F12a/AVTZ NN1	$2{,}00 \times 10^{-14}$	$1{,}73 \times 10^{-15}$	$3{,}59 \times 10^{-16}$
SCTST[c]	UCCSD(T)/ANO1	$8{,}49 \times 10^{-15}$	$3{,}66 \times 10^{-16}$	
QM[d]	WSLFH	$3{,}18 \times 10^{-15}$		
QCT[e]	UCCSD(T)/AVQZ YZCL2	$5{,}49 \pm 0{,}3 \times 10^{-15}$		
Experiment[f]		$6{,}38 \pm 0{,}5 \times 10^{-15}$		
Experiment[g]		$6{,}67 \pm 0{,}8 \times 10^{-15}$	$4{,}30 \pm 0{,}3 \times 10^{-16}$	
$OH + D_2$ reaction				
Method	PES	300 K	200 K	150 K
RPMD[a]	UCCSD(T)/AVQZ YZCL2	$1{,}16 \times 10^{-15}$	$3{,}63 \times 10^{-17}$	$2{,}36 \times 10^{-18}$
RPMD[a]	UCCSD(T)-F12a/AVTZ NN1	$1{,}50 \times 10^{-15}$	$4{,}26 \times 10^{-17}$	$2{,}94 \times 10^{-18}$
Instanton[b]	UCCSD(T)-F12a/AVTZ NN1		$7{,}46 \times 10^{-17}$	$2{,}50 \times 10^{-18}$
CVT/μ OCT[b]	UCCSD(T)-F12a/AVTZ NN1	$3{,}65 \times 10^{-15}$	$1{,}16 \times 10^{-16}$	$8{,}68 \times 10^{-18}$
QCT[e]	UCCSD(T)/AVQZ YZCL2	$1{,}40 \pm 0{,}3 \times 10^{-15}$		
Experiment[f]		$1{,}57 \pm 0{,}1 \times 10^{-15}$		

4 Conclusions

In this work, we have used ring polymer molecular dynamics (RPMD) to calculate thermal rate coefficients for the $OH + H_2$ and $OH + D_2$ reactions in the 150-2000 K temperature range. Comparison with the experimental data confirms high credibility of the RPMD method - the present thermal rates and kinetic isotope effects (as well as their temperature dependences) are within rather low deviation from the experiment. The present results also shows that two potential energy surfaces (PESs) employed in the RPMD calculations, despite different levels of theory and fitting procedures (modified shepard interpolation scheme and neural networks algorithm), provide very similar results. In our test study, we demonstrated that the agreement can be even further improved if the same level of theory is employed, at least for the present $OH + H_2$ reaction. The present results also suggest that experimental measurements of the KIEs as well as accurate quantum mechanical rate calculations for the present PESs at low temperatures (below 200 K) will be very valuable for more objective comparison with other theoretical approaches to compute thermal rate coefficients.

5 Acknowledgments

The Spanish Ministries of Science and Innovation and Economy and Competitiveness (grant CTQ2015-65033-P) is gratefully acknowledged. Y.V.S. thanks the European Regional Development Fund and the Republic of Cyprus for support through the Research Promotion Foundation (Project Cy-Tera NEA ΥΠΟΔΟΜΗ / ΣΤΡΑΤΗ/0308/31). Y.V.S. also acknowledges the support

View Article Online
DOI: 10.1039/C7CP05266A

of the COST CMTS-Action CM1401 (Our Astro-Chemical History).

View Article Online
DOI: 10.1039/C7CP05266A

References

1 J. Li, Z. Zhao, A. Kazakov, and F. Dryer, *Int. J. Chem. Kinet.*, 2004, **36**(10), 566–575.

2 R. Atkinson, D. Baulch, R. Cox, R. Hampson, J. Kerr, and J. Troe, *J. Phys. Chem. Ref. Data.*, 1992, **21**(6), 1125–1568.

3 A. Wagner and M. Graff, *Astrophys. J.*, 1987, **317**(1, 1), 423–431.

4 Y. Oba, N. Watanabe, T. Hama, K. Kuwahata, H. Hidaka, and A. Kouchi, *Astrophys. J.*, 2012, **749**(1), 1–12.

5 I. Smith and F. Crim, *Phys. Chem. Chem. Phys.*, 2002, **4**(15), 3543–3551.

6 S. Althorpe and D. Clary, *Annu. Rev. Phys. Chem.*, 2003, **54**, 493–529.

7 K. Liu, *J. Chem. Phys.*, 2006, **125**(13), 132307.

8 F. Tully and A. Ravishankara, *J. Phys. Chem.*, 1980, **84**(23), 3126–3130.

9 A. Ravishankara, J. Nicovich, R. Thompson, and F. Tully, *J. Phys. Chem.*, 1981, **85**(17), 2498–2503.

10 J. Michael and J. Sutherland, *J. Phys. Chem.*, 1988, **92**(13), 3853–3857.

11 R. Talukdar, T. Gierczak, L. Goldfarb, Y. Rudich, B. Rao, and A. Ravishankara, *J. Phys. Chem.*, 1996, **100**(8), 3037–3043.

12 R. Oldenborg, G. Loge, D. Harradine, and K. Winn, *J. Phys. Chem.*, 1992, **96**(21), 8426–8430.

13 V. Orkin, S. Kozlov, G. Poskrebyshev, and M. Kurylo, *J. Phys. Chem. A*, 2006, **110**(21), 6978–6985.

14 K.-Y. Lam, D. F. Davidson, and R. K. Hanson, *Int. J. Chem. Kinet.*, 2013, **45**(6), 363–373.

15 G. Schatz and H. Elgersma, *Chem. Phys. Lett.*, 1980, **73**(1), 21–25.

16 A. Isaacson and D. Truhlar, *J. Chem. Phys.*, 1982, **76**(3), 1380–1391.

17 U. Manthe, T. Seideman, and W. H. Miller, *J. Chem. Phys.*, 1993, **99**(12), 10078–10081.

18 U. Manthe, T. Seideman, and W. H. Miller, *J. Chem. Phys.*, 1994, **101**(6), 4759–4768.

19 M. Yang, D. Zhang, M. Collins, and S. Lee, *J. Chem. Phys.*, 2001, **115**(1), 174–178.

20 G. Wu, G. Schatz, G. Lendvay, D. Fang, and L. Harding, *J. Chem. Phys.*, 2000, **113**(8), 3150–3161.

21 A. Chakraborty and D. Truhlar, *Proc. Nat. Acad. Sciences*, 2005, **102**(19), 6744–6749.

22 E. Goldfield and S. Gray, *J. Chem. Phys.*, 2002, **117**(4), 1604–1613.

23 T. L. Nguyen, J. F. Stanton, and J. R. Barker, *J. Phys. Chem. A*, 2011, **115**(20), 5118–5126.

24 J. Chen, X. Xu, X. Xu, and D. H. Zhang, *J. Chem. Phys.*, 2013, **138**(15), 154301.

25 J. Meisner and J. Kästner, *J. Chem. Phys.*, 2016, **144**(17), 174303.

26 I. R. Craig and D. E. Manolopoulos, *J. Chem. Phys.*, 2005, **122**(8), 084106.

27 Y. V. Suleimanov, F. J. Aoiz, and H. Guo, *J. Phys. Chem. A*, 2016, **120**(43), 8488–8502.

28 R. Collepardo-Guevara, Y. V. Suleimanov, and D. E. Manolopoulos, *J. Chem. Phys.*, 2009, **130**(17), 174713.

29 R. Collepardo-Guevara, Y. V. Suleimanov, and D. E. Manolopoulos, *J. Chem. Phys.*, 2010, **133**(4), 049902.

30 Y. V. Suleimanov, R. Collepardo-Guevara, and D. E. Manolopoulos, *J. Chem. Phys.*, 2011, **134**(4), 044131.

31 R. Pérez de Tudela, F. J. Aoiz, Y. V. Suleimanov, and D. E. Manolopoulos, *J. Phys. Chem. Lett.*, 2012, **3**(4), 493–497.

32 Y. V. Suleimanov, R. P. de Tudela, P. G. Jambrina, J. F. Castillo, V. Saez-Rabanos, D. E. Manolopoulos, and F. J. Aoiz, *Phys. Chem. Chem. Phys.*, 2013, **15**, 3655–3665.

33 Y. V. Suleimanov, J. W. Allen, and W. H. Green, *Comp. Phys. Comm.*, 2013, **184**(3), 833–840.

34 J. W. Allen, W. H. Green, Y. Li, H. Guo, and Y. V. Suleimanov, *J. Chem. Phys.*, 2013, **138**(22), 221103.

35 Y. Li, Y. V. Suleimanov, J. Li, W. H. Green, and H. Guo, *J. Chem. Phys.*, 2013, **138**(9), 094307.

36 R. Pérez de Tudela, Y. V. Suleimanov, J. O. Richardson, V. Saez Rabanos, W. H. Green, and F. J. Aoiz, *J. Phys. Chem. Lett.*, 2014, **5**(23), 4219–4224.

View Article Online
DOI: 10.1039/C7CP05266A

37 E. Gonzalez-Lavado, J. C. Corchado, Y. V. Suleimanov, W. H. Green, and J. Espinosa-Garcia, *J. Phys. Chem. A*, 2014, **118**(18), 3243–3252.

38 R. P. de Tudela, Y. V. Suleimanov, M. Menendez, J. F. Castillo, and F. J. Aoiz, *Phys. Chem. Chem. Phys.*, 2014, **16**, 2920–2927.

39 J. Espinosa-Garcia, A. Fernandez-Ramos, Y. V. Suleimanov, and J. C. Corchado, *J. Phys. Chem. A*, 2014, **118**(3), 554–560.

40 Y. Li, Y. V. Suleimanov, W. H. Green, and H. Guo, *J. Phys. Chem. A*, 2014, **118**(11), 1989–1996.

41 Q. Meng, J. Chen, and D. H. Zhang, *J. Chem. Phys.*, 2015, **143**(10), 101102.

42 Y. V. Suleimanov and J. Espinosa-Garcia, *J. Phys. Chem. B*, 2016, **120**(8), 1418–1428.

43 D. J. Arseneau, D. G. Fleming, Y. Li, J. Li, Y. V. Suleimanov, and H. Guo, *J. Phys. Chem. B*, 2016, **120**(8), 1641–1648.

44 Q. Meng, J. Chen, and D. H. Zhang, *J. Chem. Phys.*, 2016, **144**(15), 154312.

45 J. Zuo, Y. Li, H. Guo, and D. Xie, *J. Phys. Chem. A*, 2016, **120**(20), 3433–3440.

46 Y. Li, Y. V. Suleimanov, and H. Guo, *J. Phys. Chem. Lett.*, 2014, **5**(4), 700–705.

47 Y. V. Suleimanov, W. J. Kong, H. Guo, and W. H. Green, *J. Chem. Phys.*, 2014, **141**(24), 244103.

48 K. M. Hickson, J.-C. Loison, H. Guo, and Y. V. Suleimanov, *J. Phys. Chem. Lett.*, 2015, **6**(21), 4194–4199.

49 S. Rampino and Y. V. Suleimanov, *J. Phys. Chem. A*, 2016, **120**(50), 9887–9893.

50 K. M. Hickson and Y. V. Suleimanov, *Phys. Chem. Chem. Phys.*, 2017, **19**(1), 480–486.

51 J. O. Richardson and S. C. Althorpe, *J. Chem. Phys.*, 2009, **131**(21), 214106.

52 T. J. H. Hele and S. C. Althorpe, *J. Chem. Phys.*, 2013, **138**(8), 084108.

53 M. A. Collins, *Theor Chem Acc*, 2002, **108**(6), 313.

54 H.-J. Werner, P. J. Knowles, G. Knizia, F. R. Manby, M. Schütz, P. Celani, W. Györffy, D. Kats, T. Korona, R. Lindh, A. Mitrushenkov, G. Rauhut, K. R. Shamasundar, T. B. Adler, R. D. Amos, A. Bernhardsson, A. Berning, D. L. Cooper, M. J. O. Deegan, A. J. Dobbyn, F. Eckert, E. Goll, C. Hampel, A. Hesselmann, G. Hetzer, T. Hrenar, G. Jansen, C. Köppl, Y. Liu, A. W. Lloyd, R. A. Mata, A. J. May, S. J. McNicholas, W. Meyer, M. E. Mura, A. Nicklass, D. P. O'Neill, P. Palmieri, D. Peng, K. Pflüger, R. Pitzer, M. Reiher, T. Shiozaki, H. Stoll, A. J. Stone, R. Tarroni, T. Thorsteinsson, and M. Wang, Molpro, version 2015.1, a package of ab initio programs, 2015.

55 E. Garcia, A. Saracibar, C. Sanchez, and A. Lagana, *Chem. Phys.*, 2005, **308**(3), 201 – 210.

56 C. H. Bennett, American Chemical Society, 1977; Vol. 46 of *Algorithms for Chemical Computations*, chapter 4, pp. 63–97.

57 D. Chandler, *J. Chem. Phys.*, 1978, **68**(6), 2959.

58 J. Kästner and W. Thiel, *J. Chem. Phys.*, 2005, **123**(14), 144104.

59 J. Kästner and W. Thiel, *J. Chem. Phys.*, 2006, **124**(23), 234106.

60 H. C. Andersen, *J. Chem. Phys.*, 1980, **72**, 2384.

61 Y. Li, Y. V. Suleimanov, M. Yang, W. H. Green, and H. Guo, *J. Phys. Chem. Lett.*, 2013, **4**(1), 48–52.

62 J. F. Stanton, *J. Phys. Chem. Lett.*, 2016, **7**(14), 2708–2713.

View Article Online
DOI: 10.1039/C7CP05266A

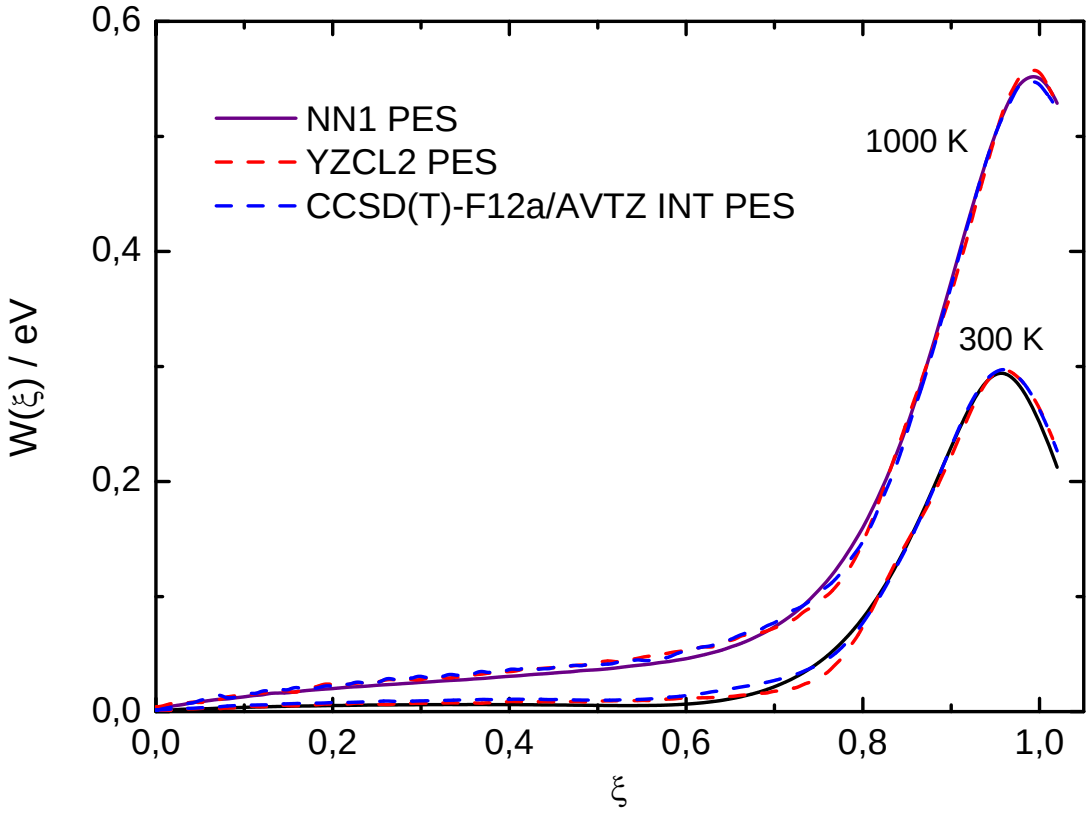

Fig. 1 RPMD potential of mean force profiles for the $OH + H_2 \rightarrow H + H_2O$ reaction.

View Article Online
DOI: 10.1039/C7CP05266A

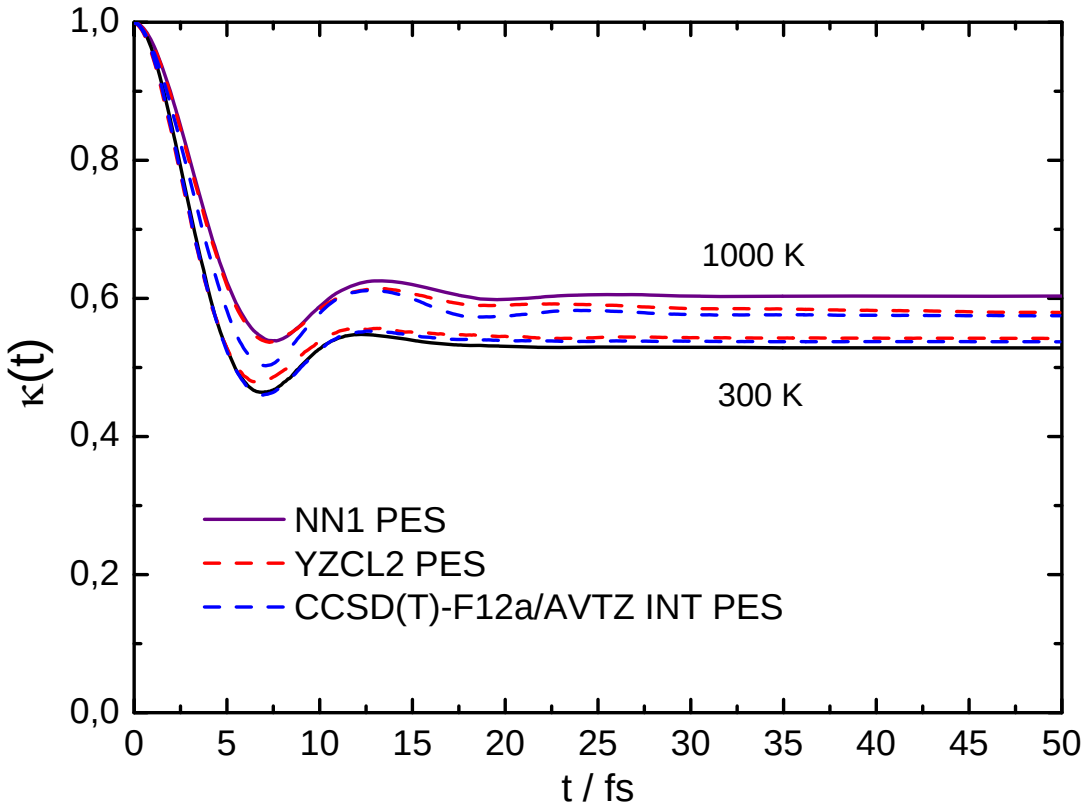

Fig. 2 RPMD time dependent transmission coefficients for the $OH + H_2 \rightarrow H + H_2O$ reaction.

View Article Online
DOI: 10.1039/C7CP05266A

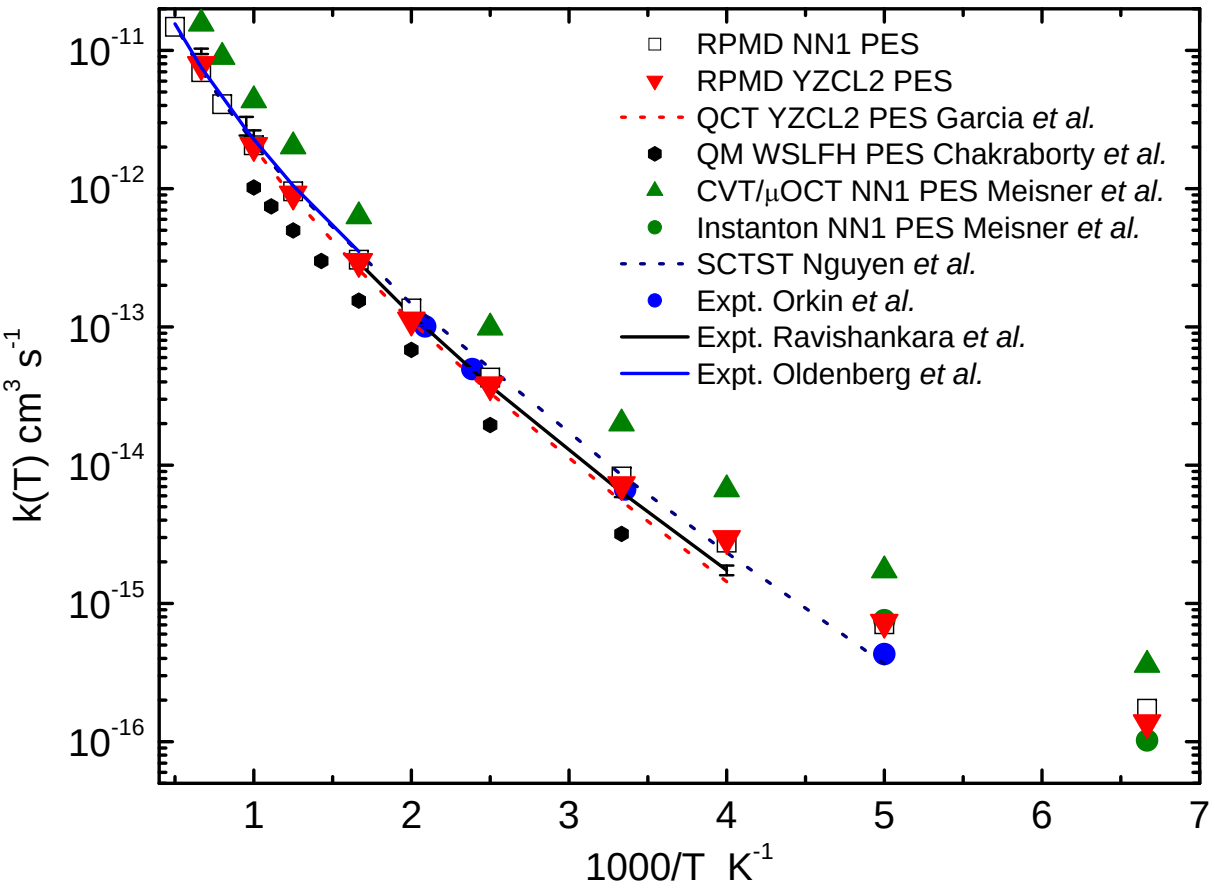

Fig. 3 Rate coefficients for the $OH + H_2$ reaction

View Article Online
DOI: 10.1039/C7CP05266A

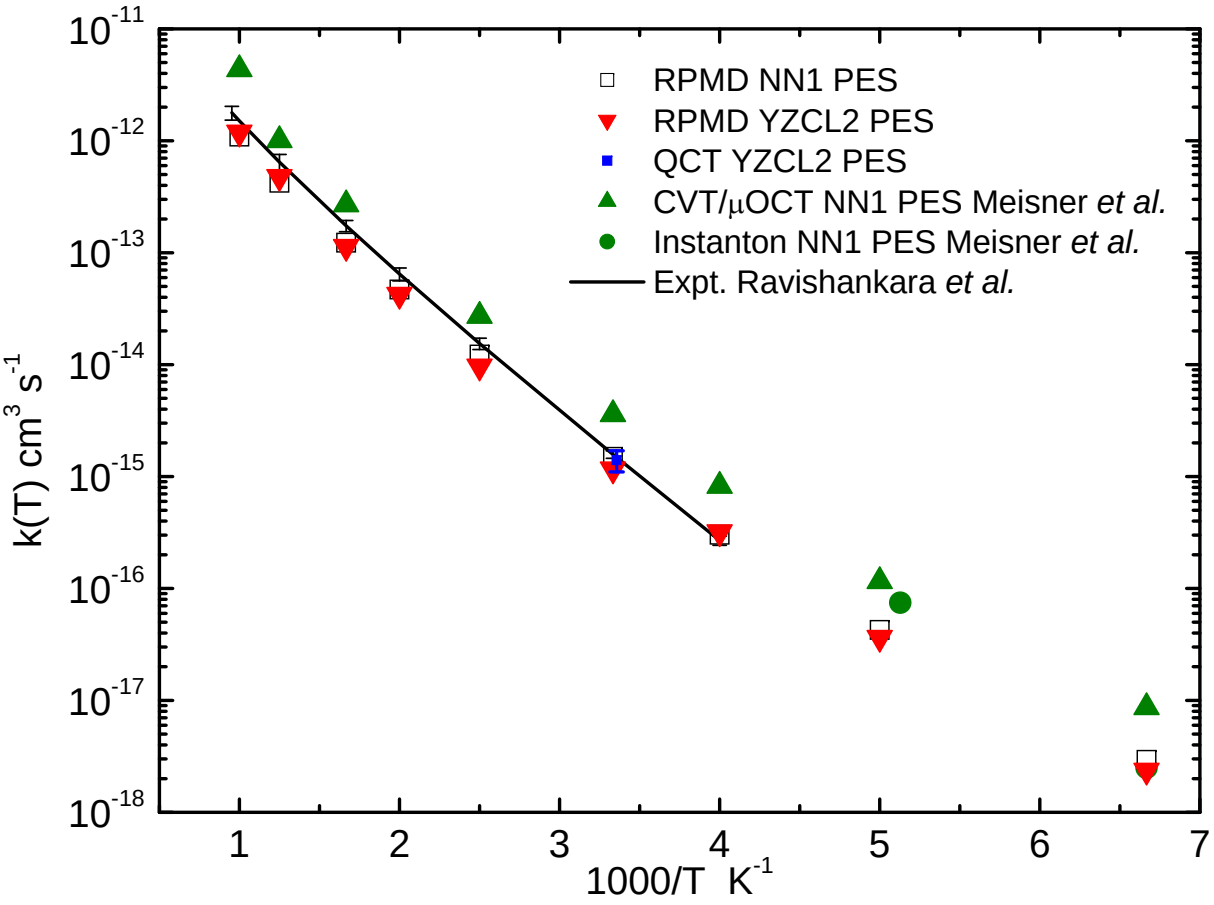

Fig. 4 Rate coefficients for the $OH + D_2$ reaction

View Article Online
DOI: 10.1039/C7CP05266A

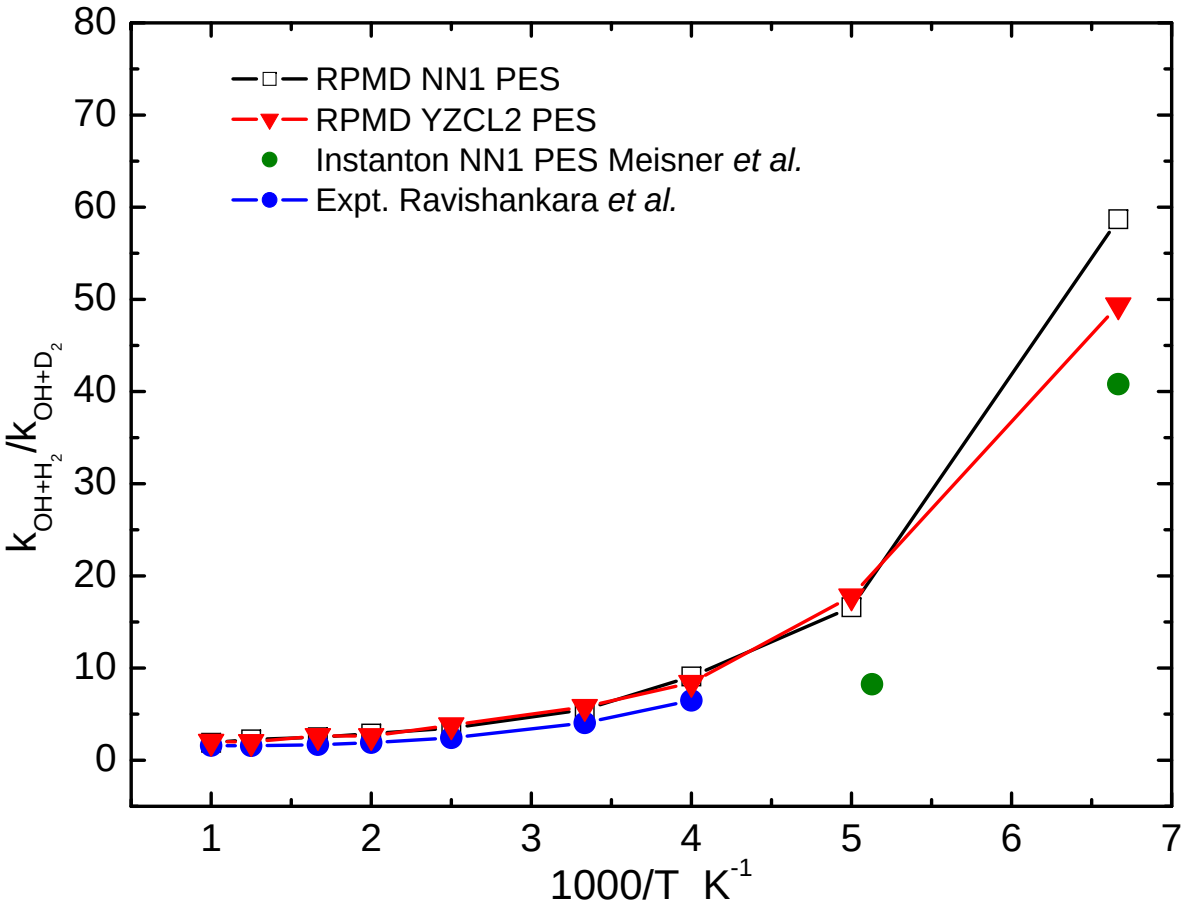

Fig. 5 Isotope branching ratio for the OH + H_2 and OH + D_2 reactions